Article

Study on the Ozone Gas Sensing Properties of rf-Sputtered Al-Doped NiO Films

Athanasios Paralikis [1,2], Emmaouil Gagaoudakis [1,*], Viktoras Kampitakis [1,2], Elias Aperathitis [1], George Kiriakidis [1] and Vassilios Binas [1,2,*]

[1] Institute of Electronic Structure & Laser, Foundation for Research and Technology (FORTH-IESL), 71100 Herakleion, Greece; ph4888@edu.physics.uoc.gr (A.P.); vkabitakis@physics.uoc.gr (V.K.); eaper@iesl.forth.gr (E.A.); kiriakid@iesl.forth.gr (G.K.)

[2] Department of Physics, University of Crete, 70013 Heraklion, Greece

[*] Correspondence: mgagas@iesl.forth.gr (E.G.); binasbill@iesl.forth.gr (V.B.); Tel.: +30-2810391272 (E.G.); +30-2810391269 (V.B.)

Featured Application: Authors are encouraged to provide a concise description of the specific application or a potential application of the work. This section is not mandatory.

Abstract: Al-doped NiO (NiO:Al) has attracted the interest of researchers due to its excellent optical and electrical properties. In this work, NiO:Al films were deposited on glass substrates by the radio frequencies (rf) sputtering technique at room temperature and they were tested against ozone gas. The Oxygen content in (Ar-O_2) plasma was varied from 2% to 4% in order to examine its effect on the gas sensing performance of the films. The thickness of the films was between 160.3 nm and 167.5 nm, while the Al content was found to be between 5.3 at% and 6.7 at%, depending on the oxygen content in plasma. It was found that NiO:Al films grown with 4% O_2 in plasma were able to detect 60 ppb of ozone with a sensitivity of 3.18% at room temperature, while the detection limit was further decreased to 10 ppb, with a sensitivity of 2.54%, at 80 °C, which was the optimum operating temperature for these films. In addition, the films prepared in 4% O_2 in plasma had lower response and recovery time compared to those grown with lower O_2 content in plasma. Finally, the role of the operating temperature on the gas sensing properties of the NiO:Al films was investigated.

Keywords: p-type sensor; Al-doped NiO; rf sputtering; ozone gas sensing

1. Introduction

Ozone (O_3) is a well-known harmful gas existing in the atmosphere as a product of photochemical reactions of Nitrogen dioxide (NO_2) and/or Volatile Organic Compounds (VOCs), which are very common environmental pollutants that come from industrial activity, cars, etc. [1]. As a result, over 80% of people live in cities where air pollution is higher than the safety limits of the World Health Organization (WHO) [2]. Taking into account that ozone is associated with various respiratory symptoms, including dyspnea, upper airway irritation, coughing, and chest tightness [1], the need of its detection in outdoor as well as indoor environments becomes of paramount importance.

Various kinds of materials, such as Metal Oxide Semiconductors (MOS) [3–5], inorganic perovskites [6], as well as hybrid perovskites [7] have been examined as gas sensing elements for ozone detection during the last decades. Among them, MOS are by far the most well studied materials for ozone gas sensing applications due to their excellent electrical and optical properties as well as the fact that they can be grown by a number of methods even at large scale [8,9]. Nickel oxide (NiO) is a p-type metal oxide semiconductor with a wide energy band gap of 3.4–3.8 eV that has interesting optoelectronic properties [10]. Thus, it can be used in UV photo-detectors [11] as an active material in photovoltaics, such as perovskite or dye-sensitized solar cells [12–16], as well as in electrochromic [17],

thermoelectric [18], and gas sensing devices for the detection of gases, such as H_2 [19,20], CH_4 [21], NO_2 [22], ethanol [23], O_3 [24], etc. Furthermore, the introduction of Aluminum (Al) atoms in the NiO structure seems to enhance its electrical as well as optical properties [25], while not affecting its gas sensing performance. As a result, Al-doped NiO films have been already tested against NO_2 [26,27], ethanol [28], CO [29], H_2, and CH_4 [30]. However, NiO:Al films have not been examined for ozone detection, according to our literature research.

In this work, rf-sputtered Al-doped NiO films were tested, for first time, against ozone. The effect of Oxygen content in Ar-O_2 plasma as well as the operating temperature on the gas sensing performance were studied. It was found that NiO:Al films have the ability to detect ozone even at room temperature, while those prepared with 4% O_2 in plasma successfully detected ozone at an ultra-low concentration of 10 ppb at 80 °C. The latter is one of the lower operating temperatures for metal oxide gas sensors.

2. Materials and Methods

2.1. Deposition Conditions

A Nordiko RFG2500 rf sputtering system was employed to grow NiO:Al films using a Ni metal target and Ar-O_2 air mixture in plasma. Two (2) Al pellets were placed on the Ni target surface for Al-doping. Both pressure and sputtering power were kept constant during deposition, being 5 mTorr and 300 W, respectively. The films were deposited on three different substrates, namely the commercial (Metrohm/DropSens) InterDigitated Transducers (glass substrate, Pt electrodes, bands/gaps = 5 μm) for sensing measurements, a piece of silicon wafer for structural characterization, and microscope glass for optical measurements. All depositions were done at room temperature (RT). The O_2 content in plasma was varied, being 2.0%, 2.8%, and 4.0% in order to examine its effect on the gas sensing characteristics of the films. After deposition, the films underwent thermal annealing at 400 °C under air for 24 h, in order to improve both their crystallinity and optical properties.

2.2. Characterization

The structure of the Al-doped NiO films was examined by the X-ray Diffraction (XRD) technique, using a PANalyticalEmpyrean diffractometer equipped with Cu-LFF as an X-Ray source, at λ = 0.15406 nm. The measurement mode was 2θ/θ varying from 20° to 90°, with a step of 0.013°/s. Using the XRD pattern the crystallite size (D) of the films was calculated according to Scherrer's Equation (1)

$$D(nm) = (0.9 \cdot \lambda)/(B \cdot \cos\theta) \qquad (1)$$

where λ is the X-ray wavelength which equals to 0.154 nm. B is the Full Width at Half Maximum (FWHM) of the corresponding peak at an angle 2θ. Moreover, the lattice constant (a_0) for the cubic structure of NiO was calculated according to Equation (2)

$$a = (h^2 + k^2 + \ell^2)^{1/2}/d \qquad (2)$$

where d is the distance between the adjacent planes in the set (hkℓ). Field Emission Surface Electron Microscopy (FESEM) was used to investigate the surface morphology of the films using a Hitachi S570 microscope, equipped with an Energy Dispersive X-ray (EDX) spectrometry system, which was employed to determine the Al at% of the NiO:Al films. Optical properties of the films were studied with a Perkin Elmer Lambda 950 UV/Vis/NIR spectrophotometer in the wavelength range of 250–2500 nm. The transmittance spectra and the corresponding Tauc plot were used in order to calculate the optical energy bandgap of the films assuming that direct transitions are permitted according to Equation (3)

$$(\alpha h v) = A \, (h v - E_g)^{1/2} \qquad (3)$$

where α is the absorption coefficient, hν the photon energy, A is a constant and E_g the optical energy bandgap. The thickness of the films was measured by using a Veeco Dektak 150 stylus profilometer.

2.3. Gas Sensing

In order to investigate the gas sensing performance in ozone, the NiO:Al films deposited on IDTs were placed in a homemade stainless steel test chamber. A mechanical pump was used to initially evacuate the chamber, while an FP-400 temperature controller was employed to regulate the operating temperature. Ozone of different concentrations was produced by an ozone analyzer (Thermo, Model 49i, Thermofisher scientific, Waltham, MA, USA). A Keithley 6517A electrometer was used to apply a constant voltage on the films and measure the electrical current variations upon the interaction between the film and the target gas. The chamber was initially evacuated at a pressure of 1 mbar. Prior to the ozone exposure, the films were treated with synthetic (dry) air for 45 min in order to be stabilized in the testing environment. After that, the films were exposed to ozone of specific concentrations for a constant time duration in which the electrical current was increased, while the recovery of the films in its initial state was done by exposing them in synthetic air for a specific time period. Both ozone and synthetic air were introduced in the chamber with a flow of 200 sccm (standard cubic centimeters per minute) regulated by mass flow controllers, while the pressure in the chamber was kept constant of 700 mbar. The whole procedure was monitored by a PC through an appropriate LabVIEW program. The sensitivity (S) of the sensor is defined by the following Equation (4)

$$S(\%) = [(I_{gas} - I_{air})/I_{air}] \cdot 100\% \tag{4}$$

where I_{gas} is the maximum value of electrical current in the presence of ozone, while I_{air} is the minimum value of electrical current in the presence of synthetic air (absence of ozone), as depicted in Figure 1. Moreover, the response time (t_{resp}) is defined as the time that is needed for the electrical current to become equal to the 90% of the value of I_{gas} in the presence of ozone, while the recovery time (t_{rec}) is defined as the required time for the electrical current to be equal to 10% of the value of I_{gas} in the absence of ozone (in the presence of synthetic air).
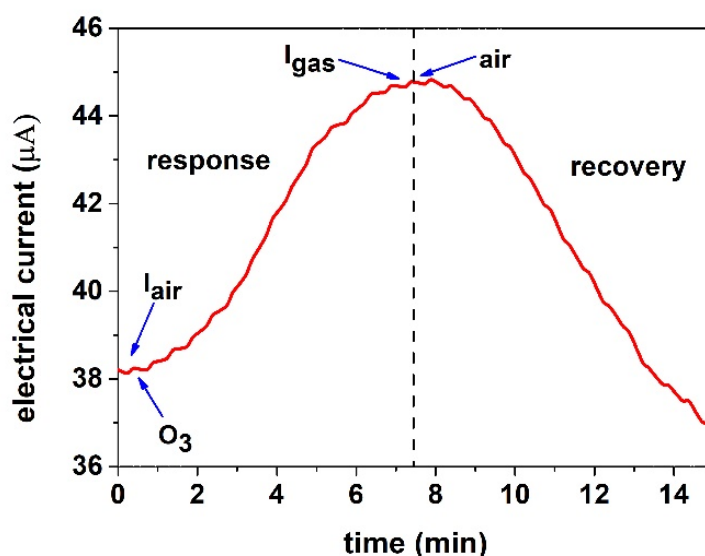

Figure 1. Typical sensing measurement of an O_3-synthetic air cycle.

All measurements were taken under the room relative humidity (RH) which was about 60%.

3. Results and Discussion

3.1. Characterization

The XRD patterns of rf-sputtered Al-doped NiO films deposited on Si substrates at room temperature with different O_2 content in plasma that underwent thermal annealing at 400 °C for 24 h are presented in Figure 2. It can be seen that all films had a polycrystalline structure with a peak of high intensity at $2\theta = 43.3°$ corresponding to a reflection from the (200) planes and two low intensity peaks at $2\theta = 36.5°$ and $62.9°$ corresponding to reflections from the (111) and (220) planes, respectively, according to JCPDS Card No. 047-1049. No peaks corresponding to other materials were found, indicating that all Al atoms were introduced in the NiO structure. Using Equation (1) for the diffraction peak with the highest intensity (200), the crystallite size of the films was calculated (Table 1) and found to be between 8.68 nm for films prepared with 2% and 2.8% O_2 in plasma and 7.89 nm for those prepared with 4% O_2 in plasma. In the case of the films prepared with 4% O_2, the decrease of the crystallite size may lead to a further increase of defect states inside the crystal structure, which can also be observed through the intensity of the main peak. In addition, the lattice constant (a_0) of the films was calculated from Equation (2) and was varied between 0.417 nm and 0.421 nm (Table 1). Both the crystallite size and lattice constant are in agreement with the values reported in the literature for Al-doped NiO films prepared by various techniques [25,31].
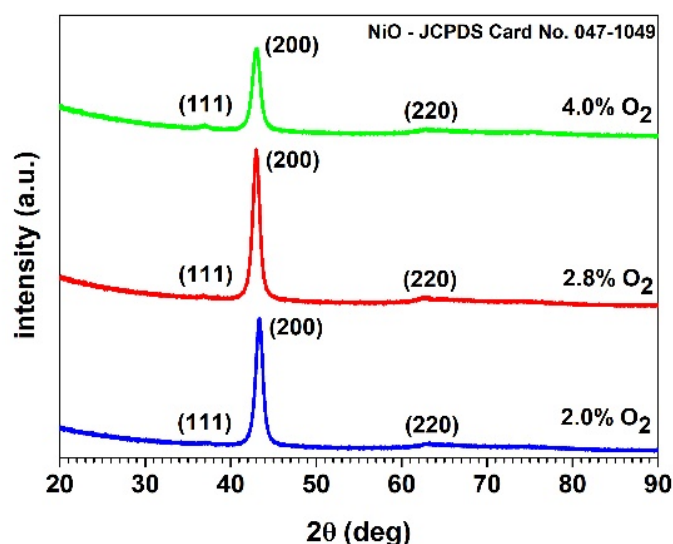

Figure 2. X-ray Diffraction (XRD) patterns of rf-sputtered NiO:Al films grown at room temperature with different O_2 content in plasma that underwent thermal annealing at 400 °C for 24 h.

Table 1. Deposition parameters, thickness (t), crystallite size (D), lattice constant (a_0), and optical energy bandgap (E_g) of rf-sputtered Al-doped NiO films.

Sample No.	% O_2 in Plasma	%at. Al	t (nm)	D (nm)	a_0 (nm)	E_g (eV)
S1749	2.0	5.3	160.3	8.68	0.417	3.66
S1746	2.8	6.5	168.7	8.68	0.421	3.65
S1743	4.0	6.7	167.5	7.89	0.420	3.66

The surface morphology of the NiO:Al films is presented in Figure 3a–c. It can be seen that all films had a smooth and uniform surface consisting of grains with a diameter of around 40 nm The increased defects on the surface of the film prepared with 4% O_2 can be also be observed.
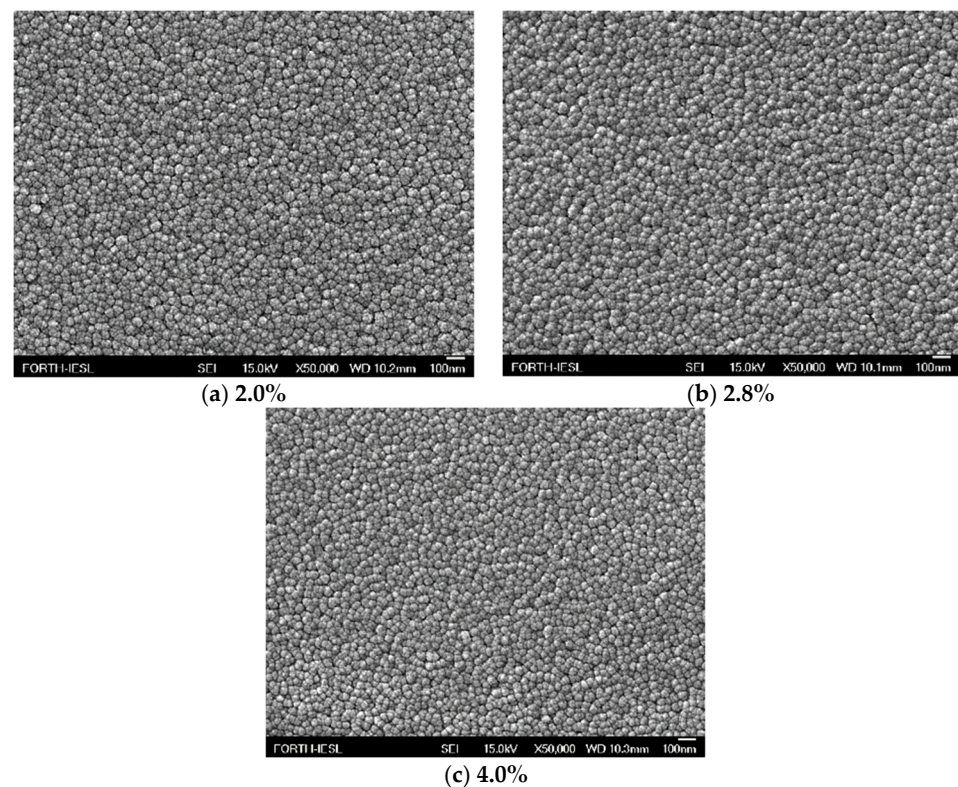
(**a**) 2.0%

(**b**) 2.8%

(**c**) 4.0%

Figure 3. SEM images of rf-sputtered NiO:Al films grown at room temperature with (**a**) 2.0%, (**b**) 2.8%, and (**c**) 4.0% O_2 content in plasma that underwent thermal annealing at 400 °C for 24 h.

The transmittance spectra of the Al-doped NiO films are shown in Figure 4. All films were highly transparent (>70%) in the visible region as well as in the near infrared one. Using Equation (3) and the Tauc plot (inset of Figure 4), the optical energy bandgap was calculated and found to be around 3.66 eV (Table 1), comparable with the values reported by Chattopadhyay et al. for Al-doped NiO films grown by the rf sputtering technique [25].
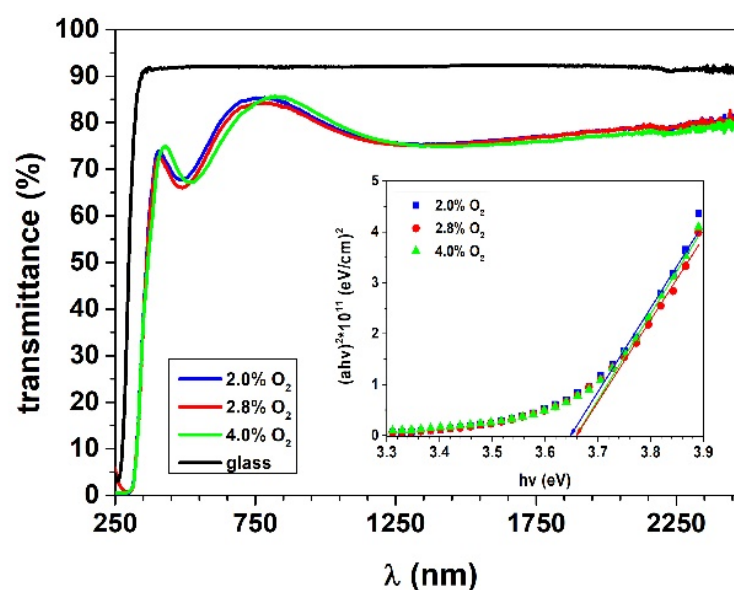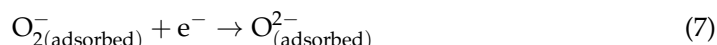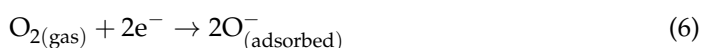

Figure 4. Transmittance spectra of rf-sputtered NiO:Al films grown at room temperature with different O_2 content in plasma that underwent thermal annealing at 400 °C for 24 h. Inset: Tauc plot to determine the optical energy band gap of the films.

3.2. Gas Sensing

The gas sensing performance of rf-sputtered Al-doped NiO films was investigated by exposing them to ozone gas with a concentration varying from 10 ppb to 3000 ppb, at operating temperatures between RT and 150 °C. The duration in ozone exposure was 5 min for films prepared with 4% O_2 in plasma and 10 min for the films prepared with 2% and 2.8% O_2 in plasma, while the recovery of the sensors was carried out by exposing them to synthetic air for 10 min and 15 min, respectively. The applied voltage was 10 V when the operating temperature equals to RT, while for the rest of the operating temperatures the applied voltage was 1 V.

A typical measurement of electrical current variation for different O_3 concentrations is presented in Figure 5. In the presence of ozone the electrical current of the film is increased reaching a maximum value, while in the absence of the target gas the electrical current of the film is decreased, as a result of its interaction with synthetic air, reaching its initial value. Moreover, it is noted that the sensor cannot be fully recovered to its initial electrical current value, especially at high concentrations (>600 ppb), probably due to residual oxidation. The gas sensing mechanism for Al-doped NiO films is the typical one for a p-type semiconductor. Thus, upon the exposure to synthetic air, Oxygen species (O, O^{2-}, etc.) are formed as a result of the O_2 adsorption on the films' surface. This is described through the following Equations (5)–(7).

$$O_{2(gas)} + e^- \rightarrow O_{2(adsorbed)}^- \tag{5}$$

$$O_{2(gas)} + 2e^- \rightarrow 2O_{(adsorbed)}^- \tag{6}$$

$$O_{2(adsorbed)}^- + e^- \rightarrow O_{(adsorbed)}^{2-} \tag{7}$$

where the kind of oxygen ions is dependent on the operating temperature (T_{oper}), being O_2^- for $T_{oper} < 100$ °C, O^- for 100 °C $< T_{oper} < 300$ °C, and O^{2-} for $T_{oper} > 300$ °C. The Oxygen species take out electrons from NiO, increasing the number of holes, leading to an increase of electrical conductivity, thus a depletion layer is formed. As a result, the height of the potential barrier at the grain boundaries is decreased and the electrical current is slightly increased. When NiO:Al films interact with ozone, which is a strongly oxidizing gas, the ozone molecules are adsorbed on the films' surface trapping the free electrons, resulting in an increase of the hole concentration as well as in a decrease of the thickness of the depletion layer. Thus, an extra increase of the electrical current is occurred [32,33].
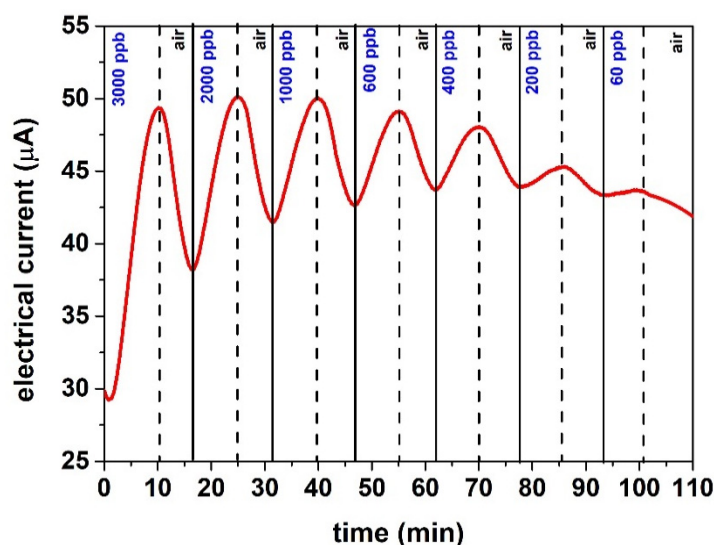

Figure 5. Electrical current variation of a NiO:Al film prepared with 4% O_2 in plasma, as a function of time for different O_3 concentrations, at 110 °C.

In Figure 6a–c the variation in sensitivity of the NiO:Al films grown with different O_2 content in plasma are shown. This was calculated by Equation (4) as a function of ozone concentration for various operating temperatures and plotted in logarithmic scale. In addition, a linear fitting has been applied confirming that the sensitivity is increased with O_3 concentration, independent of the Oxygen content in the plasma or the operating temperature. From Figure 6, it becomes clear that all films can detect the ozone gas even at an ultra-low concentration of 10 ppb. Specifically, the films prepared with 2% O_2 in plasma had a lowest detection limit of around 200 ppb with a sensitivity 1.88%, 11.31% and 38.66% at RT, 110 °C and 150 °C, respectively, while at 80 °C the lowest detection limit was 400 ppb with a sensitivity of 5.17%. Moreover, films synthesized with 2.8% O_2 in plasma had a lowest detection limit of 400 ppb [27] (sensitivity 0.84%), 200 ppb (sensitivity 6.25%), 200 ppb (sensitivity 6.94%) and 60 ppb (sensitivity 6.22%) when the operating temperature equals to RT, 80 °C, 110 °C, and 150 °C, respectively. Finally, the NiO:Al prepared with 4% O_2 in plasma appeared to have a lowest detection limit of 60 ppb (sensitivity 3.18%), 10 ppb (sensitivity 2.54%), 60 ppb (sensitivity 2.44%) and 400 ppb (sensitivity 9.02%) when the operating temperature equals to RT, 80 °C, 110 °C, and 150 °C. The detection limit of 10 ppb at 80 °C is one order of magnitude less than the one that has been reported [32] for Co_3O_4 nanobricks at almost the same working temperature (85 °C). The above mentioned values for all NiO:Al films are presented in Table 2.

Furthermore, in Figure 7 the effect of the operating temperature on gas sensing performance of the rf-sputtered NiO:Al films is shown. The films tested against 400 ppb ozone at various operating temperatures, namely RT, 80 °C, 110 °C, and 150 °C. It can be seen that films prepared with 4% O_2 in plasma appeared to have the best sensitivity at 80 °C, while the rest of them showed a maximum sensitivity at 150 °C. This can be attributed to both less Al content and smaller crystallite size of the films grown with 4% O_2 in plasma compared to the others, which also leads to a further decrease of the defect states that can reduce the adsorption energy of the O_3 gas molecules [34]. In addition, the operating temperature of 80 °C is one of the lowest that has been reported for ultra-low ozone concentration (10 ppb) [4,32].

Finally, the response and recovery time of the NiO:Al films for each operating temperature were calculated and presented in Figure 8a–c. Films grown with 2% and 2.8% O_2 in plasma had a response time between 400 s and 800 s, depending on both operating temperature and ozone concentration, while for those prepared with 4% O_2 in plasma the response time was ranging from 150 s to 500 s. In the same way, the recovery time for the former films was between 400 s and 900 s, while it was varied from 200 s to 600 s for films grown with 4% O_2 in plasma. It should be noticed that the Al: NiO films grown with 4% O_2 in plasma showed the best response and the recovery time equals to 189.6 s and 243.6 s, respectively, against 10 ppb ozone at an operating temperature of 80 °C. The response time values of Al: NiO films are higher than those in other reported works, while the recovery time values are comparable to those reported in the literature [4,32,34–38]. However, most of these sensors work at higher temperatures and/or have a higher concentration detection limit than those presented in this work.
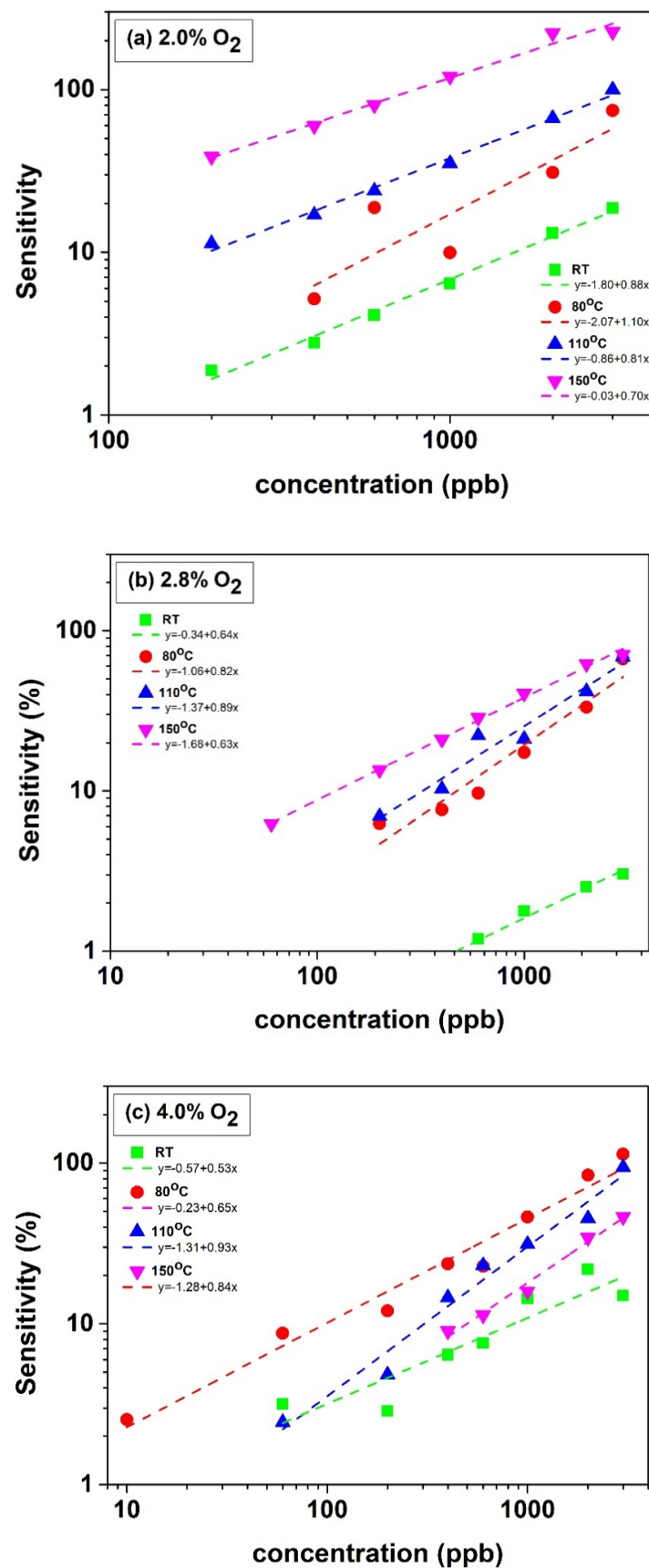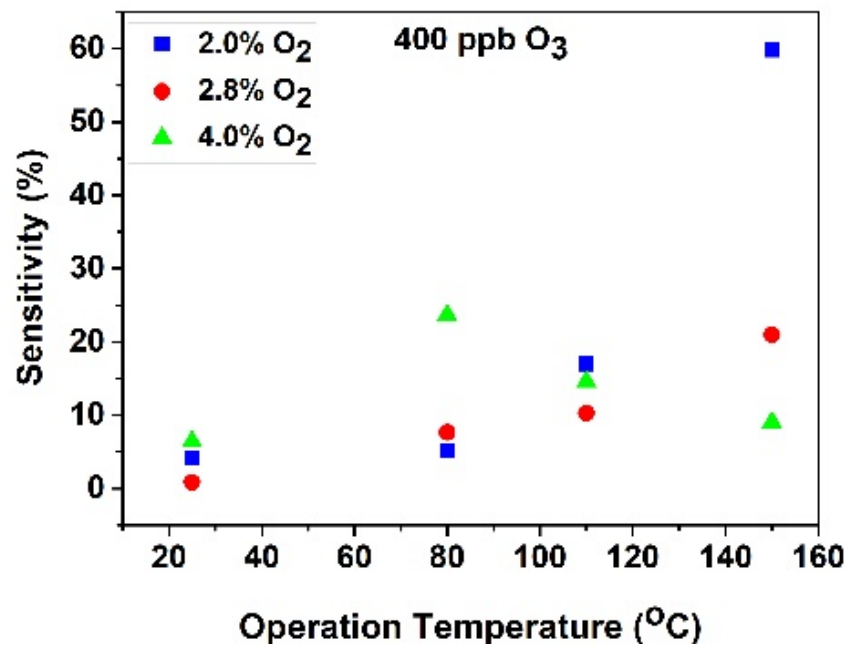
Figure 6. Sensitivity on different ozone concentrations at various operating temperatures of rf-sputtered NiO:Al with (**a**) 2.0%, (**b**) 2.8%, and (**c**) 4.0% O_2 in plasma. A linear fitting plot has been applied.

Table 2. Deposition parameters, temperature of operation (°C), minimum detection concentration (ppb), and sensitivity (S) of rf-sputtered Al-doped NiO films.

Sample No.	% O_2 in Plasma	T_{oper} (°C)	Minimum Detected Concentration (ppb)	S (%)
S1749	2.0	RT	213	1.88
		80	393	5.17
		110	213	11.31
		150	207	38.66
S1746	2.8	RT	393	0.84
		80	212	6.25
		110	215	6.94
		150	67	6.22
S1743	4.0	RT	58	3.18
		80	13	2.54
		110	59	2.44
		150	330	9.02

Figure 7. Sensitivity of rf-sputtered NiO:Al films grown with different O_2 content in plasma as a function of operating temperature.
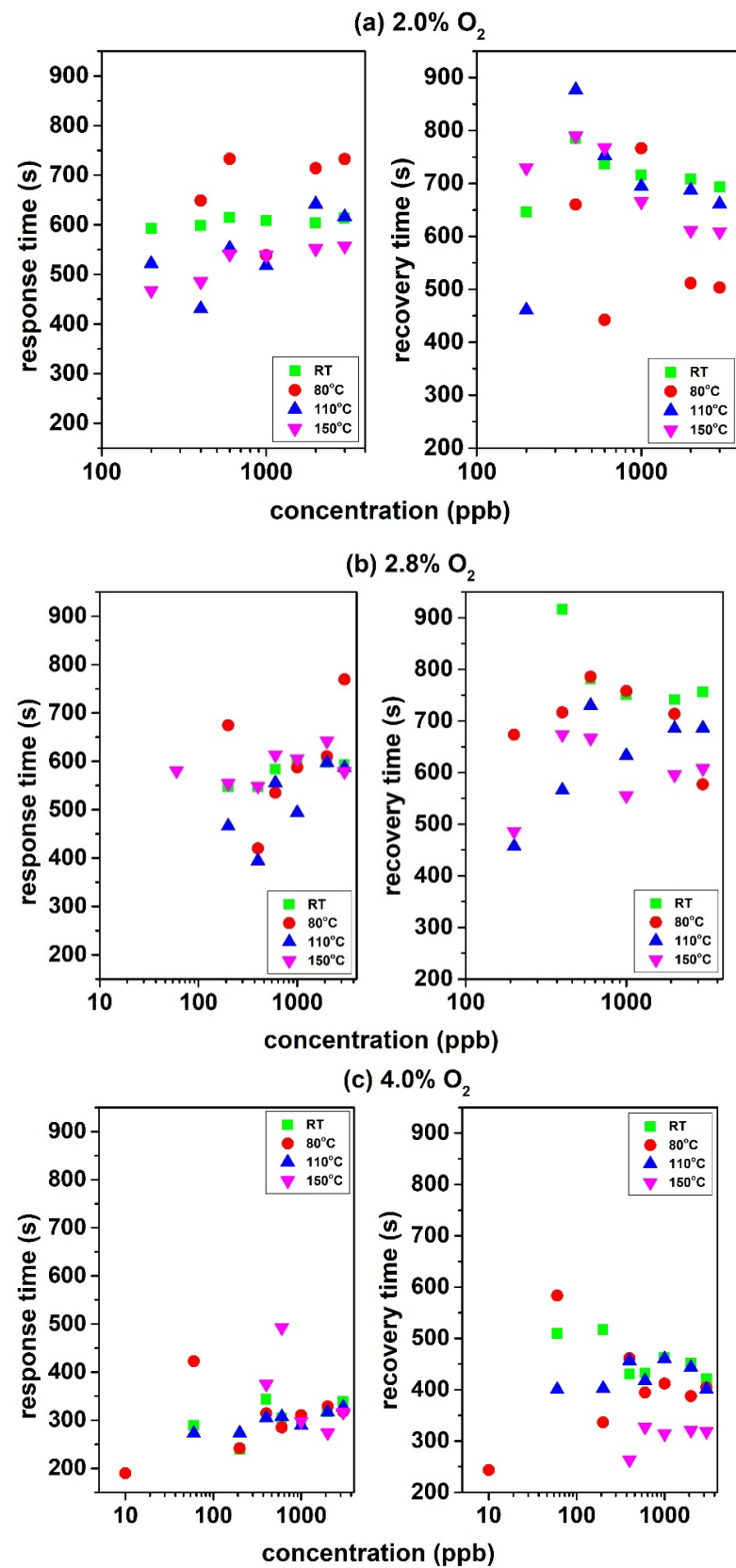
Figure 8. Response and recovery times at different operating temperatures of rf-sputtered NiO:Al with (**a**) 2.0%, (**b**) 2.8%, and (**c**) 4.0% O_2 in plasma as a function of ozone concentrations.

4. Conclusions

Al-doped NiO films were grown by the rf sputtering technique with different oxygen contents in Ar-O_2 plasma, i.e., 2%, 2.8%, and 4%, at room temperature. All films were polycrystalline as revealed by the XRD technique, while their surface was smooth as was confirmed by Scanning Electron Microscopy. Moreover, all films were highly transparent, showing a transmittance of more than 70% in the visible spectrum. The gas sensing performance of the films against ozone was studied at different operating temperatures, namely 25 °C, 80 °C, 110 °C, and 150 °C. All films were sensitive to ozone of different concentrations. Specifically, films grown with 4% O_2 in plasma were able to detect ozone at an ultra-low concentration of 10 ppb at a low operating temperature of 80 °C. Thus NiO:Al films can be potentially used as a sensing element for ozone gas sensors.

Institutional Review Board Statement: Not applicable.

Informed Consent Statement: Not applicable.

Data Availability Statement: Not applicable.

Conflicts of Interest: The authors declare no conflict of interest.

References

1. Huangfu, P.; Atkinson, R. Long-term exposure to NO_2 and O_3 and all-cause and respiratory mortality: A systematic review and meta-analysis. *Environ. Int.* **2020**, *144*, 105998. [CrossRef]
2. Barkjohn, K.K.; Norris, C.; Cui, X.; Fang, L.; Zheng, T.; Schauer, J.J.; Li, Z.; Zhang, Y.; Black, M.; Zhang, J.; et al. Real-time measurements of PM 2.5 and ozone to assess the effectiveness of residential indoor air filtration in Shanghai homes. *Indoor Air* **2021**, *31*, 74–87. [CrossRef]
3. Bejaoui, A.; Guerin, J.; Zapien, J.; Aguir, K. Theoretical and experimental study of the response of CuO gas sensor under ozone. *Sens. Actuators B Chem.* **2014**, *190*, 8–15. [CrossRef]
4. Rocha, L.; Foschini, C.; Silva, C.; Longo, E.; Simões, A. Novel ozone gas sensor based on ZnO nanostructures grown by the microwave-assisted hydrothermal route. *Ceram. Int.* **2016**, *42*, 4539–4545. [CrossRef]
5. Petromichelaki, E.; Gagaoudakis, E.; Moschovis, K.; Tsetseris, L.; Anthopoulos, T.D.; Kiriakidis, G.; Binas, V. Highly sensitive and room temperature detection of ultra-low concentrations of O_3 using self-powered sensing elements of Cu_2O nanocubes. *Nanoscale Adv.* **2019**, *1*, 2009–2017. [CrossRef]
6. Brintakis, K.; Gagaoudakis, E.; Kostopoulou, A.; Faka, V.; Argyrou, A.; Binas, V.; Kiriakidis, G.; Stratakis, E. Ligand-free all-inorganic metal halide nanocubes for fast, ultra-sensitive and self-powered ozone sensors. *Nanoscale Adv.* **2019**, *1*, 2699–2706. [CrossRef]
7. Kakavelakis, G.; Gagaoudakis, E.; Petridis, K.; Petromichelaki, V.; Binas, V.; Kiriakidis, G.; Kymakis, E. Solution Processed CH3NH3PbI3–xClxPerovskite Based Self-Powered Ozone Sensing Element Operated at Room Temperature. *ACS Sens.* **2018**, *3*, 135–142. [CrossRef] [PubMed]
8. Wetchakun, K.; Samerjai, T.; Tamaekong, N.; Liewhiran, C.; Siriwong, C.; Kruefu, V.; Wisitsoraat, A.; Tuantranont, A.; Phanichphant, S. Semiconducting metal oxides as sensors for environmentally hazardous gases. *Sens. Actuators B Chem.* **2011**, *160*, 580–591. [CrossRef]
9. Moseley, P.T. Progress in the development of semiconducting metal oxide gas sensors: A review. *Meas. Sci. Technol.* **2017**, *28*, 082001. [CrossRef]
10. Reddy, A.M.; Reddy, A.S.; Lee, K.-S.; Reddy, P.S. Effect of oxygen partial pressure on the structural, optical and electrical properties of sputtered NiO films. *Ceram. Int.* **2011**, *37*, 2837–2843. [CrossRef]
11. Echresh, A.; Chey, C.O.; Shoushtari, M.Z.; Khranovskyy, V.; Nour, O.; Willander, M. UV photo-detector based on p-NiO thin film/n-ZnO nanorods heterojunction prepared by a simple process. *J. Alloys Compd.* **2015**, *632*, 165–171. [CrossRef]

12. Bonomo, M.; Naponiello, G.; Venditti, I.; Zardetto, V.; Di Carlo, A.; Dini, D. Electrochemical and Photoelectrochemical Properties of Screen-Printed Nickel Oxide Thin Films Obtained from Precursor Pastes with Different Compositions. *J. Electrochem. Soc.* **2016**, *164*, H137–H147. [CrossRef]

13. Di Girolamo, D.; Matteocci, F.; Piccinni, M.; Di Carlo, A.; Dini, D. Anodically electrodeposited NiO nanoflakes as hole selective contact in efficient air processed p-i-n perovskite solar cells. *Sol. Energy Mater. Sol. Cells* **2020**, *205*, 110288. [CrossRef]

14. Di Girolamo, D.; Di Giacomo, F.; Matteocci, F.; Marrani, A.G.; Dini, D.; Abate, A. Progress, highlights and perspectives on NiO in perovskite photovoltaics. *Chem. Sci.* **2020**, *11*, 7746–7759. [CrossRef]

15. Bonomo, M.; Dini, D.; Decker, F. Electrochemical and Photoelectrochemical Properties of Nickel Oxide (NiO) With Nanostructured Morphology for Photoconversion Applications. *Front. Chem.* **2018**, *6*, 601. [CrossRef] [PubMed]

16. Bonomo, M.; Sheehan, S.; Dowling, D.P.; Gontrani, L.; Dini, D. First Evidence of Electrode Reconstruction in Mesoporous NiO After Operation as Photocathode of Dye-Sensitized Solar Cells. *ChemistrySelect* **2018**, *3*, 6729–6736. [CrossRef]

17. Sahu, D.; Lee, Y.-H.; Wu, T.-J.; Wang, S.-C.; Huang, J.-L. Synthesis and electrochromic property improvement of NiO films for device applications. *Thin Solid Films* **2020**, *707*, 138097. [CrossRef]

18. Sarkar, K.; Debnath, A.; Deb, K.; Bera, A.; Saha, B. Effect of NiO incorporation in charge transport of polyaniline: Improved polymer based thermoelectric generator. *Energy* **2019**, *177*, 203–210. [CrossRef]

19. Nakate, U.T.; Ahmad, R.; Patil, P.; Yu, Y.; Hahn, Y.-B. Ultra thin NiO nanosheets for high performance hydrogen gas sensor device. *Appl. Surf. Sci.* **2020**, *506*, 144971. [CrossRef]

20. Gagaoudakis, E.; Michail, G.; Kampylafka, V.; Tsagaraki, K.; Aperathitis, E.; Moschovis, K.; Binas, V.; Kiriakidis, G. Room Temperature p-Type NiO Nanostructure Thin Film Sensor for Hydrogen and Methane Detection. *Sens. Lett.* **2017**, *15*, 663–667. [CrossRef]

21. Zhang, S.; Li, Y.; Sun, G.; Zhang, B.; Wang, Y.; Cao, J.; Zhang, Z. Enhanced methane sensing properties of porous NiO nanaosheets by decorating with SnO_2. *Sens. Actuators B Chem.* **2019**, *288*, 373–382. [CrossRef]

22. Urso, M.; Leonardi, S.G.; Neri, G.; Petralia, S.; Conoci, S.; Priolo, F.; Mirabella, S. Room temperature detection and modelling of sub-ppm NO_2 by low-cost nanoporous NiO film. *Sens. Actuators B Chem.* **2020**, *305*, 127481. [CrossRef]

23. Su, C.; Zhang, L.; Han, Y.; Ren, C.; Chen, X.; Hu, J.; Zeng, M.; Hu, N.; Su, Y.; Zhou, Z.; et al. Controllable synthesis of crescent-shaped porous NiO nanoplates for conductometric ethanol gas sensors. *Sens. Actuators B Chem.* **2019**, *296*, 126642. [CrossRef]

24. Demin, V.S.; Krasovskii, A.N.; Lyudchik, A.M.; Pokatashkin, V.I.; Grigorishin, I.L.; Kudanovich, O.N. Measurement of ozone over a wide range of concentrations using semiconductor NiO gas sensors. *Meas. Tech.* **2008**, *51*, 1038–1044. [CrossRef]

25. Nandy, S.; Maiti, U.N.; Ghosh, C.K.; Chattopadhyay, K.K. Enhanced p-type conductivity and band gap narrowing in heavily Al doped NiO thin films deposited by RF magnetron sputtering. *J. Phys. Condens. Matter* **2009**, *21*, 115804. [CrossRef]

26. Wang, S.; Huang, D.; Xu, S.; Jiang, W.; Wang, T.; Hu, J.; Hu, N.; Su, Y.; Zhang, Y.; Yang, Z. Two-dimensional NiO nanosheets with enhanced room temperature NO_2 sensing performance via Al doping. *Phys. Chem. Chem. Phys.* **2017**, *19*, 19043–19049. [CrossRef] [PubMed]

27. Kampitakis, V.; Gagaoudakis, E.; Zappa, D.; Comini, E.; Aperathitis, E.; Kostopoulos, A.; Kiriakidis, G.; Binas, V. Highly sensitive and selective NO_2 chemical sensors based on Al doped NiO thin films. *Mater. Sci. Semicond. Process.* **2020**, *115*, 105149. [CrossRef]

28. Wang, C.; Cui, X.; Liu, J.; Zhou, X.; Cheng, X.; Sun, P.; Hu, X.; Li, X.; Zheng, J.; Lu, G. Design of Superior Ethanol Gas Sensor Based on Al-Doped NiO Nanorod-Flowers. *ACS Sens.* **2016**, *1*, 131–136. [CrossRef]

29. Abdul-Hussein, Y.M.; Ali, H.J.; Latif, L.A.; Abdulsattar, M.A.; Fadhel, H.M. Preparation of Al-Doped NiO Thin Films by Spray Pyrolysis Technique for CO Gas Sensing. *J. Adv. Pharm. Educ. Res.* **2019**, *9*, 1–6.

30. Gagaoudakis, E.; Michail, G.; Katerinopoulou, D.; Moschovis, K.; Iliopoulos, E.; Kiriakidis, G.; Binas, V.; Aperathitis, E. Transparent p-type NiO:Al thin films as room temperature hydrogen and methane gas sensors. *Mater. Sci. Semicond. Process.* **2020**, *109*, 104922. [CrossRef]

31. Siddique, M.N.; Ahmed, A.; Tripathi, P. Electric transport and enhanced dielectric permittivity in pure and Al doped NiO nanostructures. *J. Alloys Compd.* **2018**, *735*, 516–529. [CrossRef]

32. Liu, L.; Li, T.; Yi, Z.; Chi, F.; Lin, Z.; Zhang, X.; Xu, K. Conductometric ozone sensor based on mesoporous ultrafine Co3O4 nanobricks. *Sens. Actuators B Chem.* **2019**, *297*, 126815. [CrossRef]

33. Mokoena, T.P.; Swart, H.C.; Motaung, D.E. A review on recent progress of p-type nickel oxide based gas sensors: Future perspectives. *J. Alloys Compd.* **2019**, *805*, 267–294. [CrossRef]

34. Sun, Q.; Wu, Z.; Cao, Y.; Guo, J.; Long, M.; Duan, H.; Jia, D. Chemiresistive sensor arrays based on noncovalently functionalized multi-walled carbon nanotubes for ozone detection. *Sens. Actuators B Chem.* **2019**, *297*, 126689. [CrossRef]

35. Onofre, Y.J.; Catto, A.C.; Bernardini, S.; Fiorido, T.; Aguir, K.; Longo, E.; Mastelaro, V.R.; da Silva, L.F.; de Godoy, M.P. Highly selective ozone gas sensor based on nanocrystalline $Zn_{0.95}Co_{0.05}O$ thin film obtained via spray pyrolysis technique. *Appl. Surf. Sci.* **2019**, *478*, 347–354. [CrossRef]

36. Wu, C.-H.; Jiang, G.-J.; Chang, K.-W.; Deng, Z.-Y.; Li, Y.-N.; Chen, K.-L.; Jeng, C.-C. Analysis of the Sensing Properties of a Highly Stable and Reproducible Ozone Gas Sensor Based on Amorphous In-Ga-Zn-O Thin Film. *Sensors* **2018**, *18*, 163. [CrossRef] [PubMed]

37. Catto, A.C.; Da Silva, L.F.; Ribeiro, C.; Bernardini, S.; Aguir, K.; Longo, E.; Mastelaro, V.R. An easy method of preparing ozone gas sensors based on ZnO nanorods. *RSC Adv.* **2015**, *5*, 19528–19533. [CrossRef]

38. Joshi, N.; Da Silva, L.F.; Jadhav, H.; M'Peko, J.-C.; Torres, B.B.M.; Aguir, K.; Mastelaro, V.R.; Oliveira, O.N. One-step approach for preparing ozone gas sensors based on hierarchical $NiCo_2O_4$ structures. *RSC Adv.* **2016**, *6*, 92655–92662. [CrossRef]